

---

## Chapter 21<sup>1</sup>

# Optical fibre based monitoring of high voltage power equipment

G.R. Jones

---

### 21.1 Introduction

Optical fibre usage has grown mainly in the domain of the telecommunications industry, but is now emerging in the fields of data communications, community antenna television (CATV) and control applications, where the high inherent bandwidth available and relative immunity to electromagnetic interference (EMI) is becoming increasingly advantageous. Fibre, especially in digital communications, overcomes, for example, the problems of differential earth potentials between locations, and is largely immune to lightning strikes and other electromagnetic interference. As the data transfer rates of local area networks increase, fibre becomes increasingly attractive and more economically viable. In terms of pence per metre per unit bandwidth, fibre as a transmission medium is the obvious choice for an increasing number of applications.

In the domain of electrical power systems optical fibre technology (with the above advantages) has the scope of being used for a variety of purposes. The adoption of telecommunications technology is already well advanced and the realisation of reliable optical data transmission for protection and control is being convincingly demonstrated. Furthermore, research into optical fibre-based parameter sensing has reached the stage that properly engineered systems are becoming available whose integration into an optical fibre network should eventually lead to a purely optical monitoring and transmission system.

<sup>1</sup> Section 21.2 is based upon part of Chapter 27 of the *Electrical Engineer's Reference Book, 15th edition* (edited by Jones, Laughton and Say), published by Butterworth-Heinemann, 1993, and appears with permission.

## 21.2 Optical fibre fundamentals

### 21.2.1 Optical propagation in fibres: ray theory

Light propagation through an optical fibre depends on total internal reflection at the interface between two transparent materials with high and low refractive indices. Figure 21.1 shows that, as a ray approaches a boundary within a transparent medium, it can be totally internally reflected at the high-low refractive index interface, and is guided along the high refractive index medium. As the angle at which the approaching ray increases, a critical value  $\theta_2$  may be reached beyond which light 'leaks' out of both media.

The most basic type of optical fibre can be developed from the above principle by using a cylindrical geometry: rays beyond the critical angle are trapped within the fibre core and travel down the fibre.

### 21.2.2 Acceptance angle and numerical aperture

Consider the fibre illustrated in Figure 21.1, with a circular core of diameter  $d$ , and a uniform refractive index  $n_1$ , surrounded by a cladding layer of uniform refractive index  $n_2$ . Light launched into the core at angles  $\theta_1$  will be propagated within the core at angles  $\theta_3$ , up to a maximum value  $\theta_2$  to the axis. Light at angles greater than  $\theta_2$  will not be internally reflected and will be refracted into the cladding. The maximum launch or acceptance angle  $\theta_1$  can be expressed as a function of the numerical aperture (NA), where:

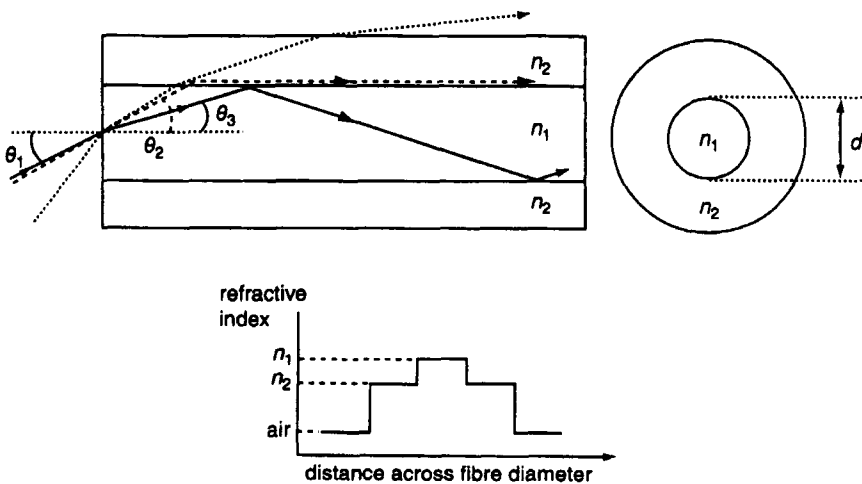


Figure 21.1 Ray diagram for multimode step index fibre

$$NA = (n_1^2 - n_2^2)^{1/2} = \sin\theta_1 = n_1 \sin\theta_2 \quad (21.1)$$

Note that reciprocity dictates that what is true for light entering the core of a fibre is also true for light exiting. The fibre core diameter ( $d$ ), the  $NA$  and the operating wavelength ( $\lambda$ ) are often used together in a single parameter, known as the normalised frequency, waveguide parameter or fibre parameter ( $V$ ), which is of importance in characterising all fibres:

$$V = \frac{\pi d}{\lambda} NA \quad (21.2)$$

### 21.2.3 Basic fibre types, modes, mode conversion and bandwidth

Waveguide theory shows that the total number of modes which can be sustained in a step index fibre is given by  $N \approx V^2/2$ . Modes can be visualised as rays propagating at differing angles to the fibre core. Discrete and definable modes only can propagate because of the geometric constraints of the fibre, and are analogous to modes in hollow metallic waveguides used at microwave frequencies (ca. 1–100 GHz). Typical multimode fibres, with core diameters of 50–200  $\mu\text{m}$ , propagate 100–1000 modes. It is not necessary for the general user of fibres to understand the mathematics of propagation in detail.

In a multimode step index fibre (Figure 21.2(a)), however careful one is to launch a single mode, conversion between modes or ray angles is inevitable because of bending and fibre imperfections. This is a great drawback for such fibres, because different modes travel at different

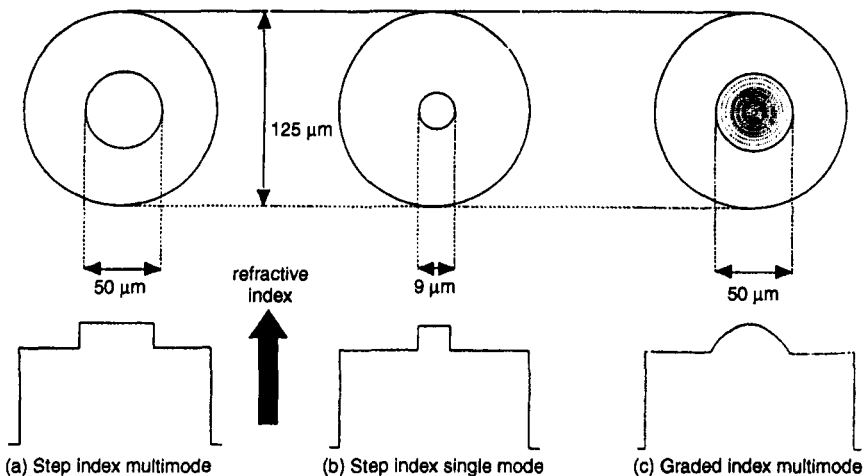


Figure 21.2 Refractive index profiles (typical dimensions shown)

speeds down the fibre, causing different arrival times at the receiving end. The difference in transit time between the extreme ray paths for a multi-mode step index fibre of length  $L$  is given by

$$\Delta T_{\text{intermodal}} = \frac{L}{c} (n_1 - n_2) \quad (21.3)$$

where  $c$  is the velocity of light. The difference in transit times causes a sharp pulse of launched light to become spread at the distant end, limiting the bandwidth of a system. Typically, for an all-silica based fibre of  $NA \approx 0.2$ , pulse spreading is of the order of 50 ns/km, and is inversely proportional to the length of the system; the longer the system, the lower the bandwidth.

As  $V$  is reduced, fewer guided rays or modes can be supported, and when  $V < 2.405$ , only a single waveguide mode can propagate. Such single-mode fibres have a core diameter which is comparable with the wavelength of light ( $d$  is commonly 8–10  $\mu\text{m}$  for telecommunications fibres – see Figure 21.2(b)), making fibre-fibre and fibre-device interconnection more difficult and generally less efficient than for multimode fibres. Single- or mono-mode fibres have, however, become the predominant type for most telecommunications links over 1 km or so, and are generally used at 1300 nm and 1550 nm wavelengths where attenuation is low and sources and detectors are available. Intermodal dispersion does not occur and bandwidths can be very high.

Note that fibre which is single mode at, say, 1300 nm will not necessarily be single-mode at 850 nm or below.  $V$  increases as the wavelength decreases, and will generally be greater than 2.405 at 850 nm. A wavelength known as the cut-off wavelength is an important manufacturing parameter defining the onset of multimode behaviour.

Simple ray optics do not describe energy through a single-mode fibre; it is difficult to depict a single ray being guided. Mathematical modelling of single- and multimode fibre is achieved by solving Maxwell's equations with boundary conditions defined by fibre geometry and wavelength. This involves Bessel functions and is beyond the scope of this introduction. One of the important results of mathematical modelling is that optical power is not confined to the core alone, but extends appreciably into the cladding region – the power distribution is approximately Gaussian. The extent of cladding penetration is dependent primarily on refractive index difference and wavelength.

A fibre-type intermediate between step index multimode and step index single-mode was developed to overcome bandwidth and connection difficulties; this is the graded index fibre. Here, the radial refractive index profile is graded, and the paths of rays travelling along the fibre are curved rather than linear as in Figure 21.1 because the rays are continuously rather than abruptly refracted. Rays which travel nearer the

core-cladding boundary are in a region of lower refractive index, and travel faster than those in the denser central core area. The overall effect, given an appropriate refractive index profile, is that rays travelling along different paths arrive at the fibre end at approximately the same time. The exact index profile to minimise dispersion effects is dependent on the composition of the fibre and the operating wavelength, but is approximately parabolic.

Graded index fibres dominated the telecommunications market in the early 1980s until single-mode technology was perfected. Single-mode fibre is used almost universally in telecommunications, but multimode fibre has realised a new lease of life in emerging high speed (ca. 100 megabits per second (MBps) local area networks, and 62.5/125 (core/cladding diameters in  $\mu\text{m}$ ) fibre has been specified as the first choice for the ANSI X3T9.5 committee FDDI (Fibre Distributed Data Interface) standard.

One other fundamental dispersion mechanism operates in all fibres. This is material dispersion, which is the result of light of different wavelengths (from an LED and even a narrower linewidth laser source) travelling at different velocities down the fibre, and which predominates in single-mode fibres. The speed of light propagating in the fibre is inversely proportional to the refractive index of the propagating medium, and the refractive index of silica drops from 1.46 to 1.44 between 600 and 200nm, approximately. The variation of the material dispersion parameter  $M(\lambda)$  with respect to wavelength is given by

$$M(\lambda) = -\frac{\lambda}{c} \frac{d^2 n_1}{d\lambda^2} \text{ (ps/nm/km)} \quad (21.4)$$

and is shown for silica in Figure 21.3. Pulse broadening in a particular case

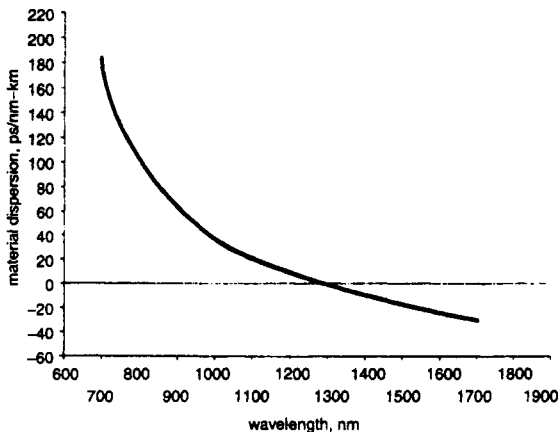


Figure 21.3 Material dispersion against wavelength for silica

can be calculated by multiplying the value of  $M(\lambda)$  by both the length of fibre in question and the linewidth of the source in nanometres. An LED source, for example, operating at 850nm and with a linewidth of 40 nm will give pulse spreading of some 4 ns/km, and this spreading may be significantly reduced by using a laser source with much reduced linewidth of typically 4 nm or less. The bandwidth-length product is generally specified for multimode fibre in the region of 850 nm, called the first window (where sources and detectors were available, and fibre losses were acceptable at approximately 3 dB/km or greater), but second window systems operate at 1300 nm and can exploit the dispersion zero to give high bandwidths. Also, at 1300 nm, losses can be substantially below 1 dB/km, giving far greater transmission distances before regeneration is required. A third window at 1550 nm, at which attenuation can be less than 0.2dB/km, is now in common telecommunications use. Figure 21.4 shows nominal attenuation against wavelength for all-silica fibre, and indicates operating windows.

By modifying the chemical composition of single-mode fibre, and the geometry of the core and cladding, the zero of  $M(\lambda)$  can be moved to 1550 nm, but this is achieved only at the expense of an attenuation penalty and is not common practice. (High bandwidth systems are generally achieved by using very narrow spectral linewidth lasers.)

The above treatise generally refers to all-silica fibres – these are by far the most widely used, as they are deployed in the telecommunications industry. The two other common types are plastic-clad-silica (PCS) and all-plastic fibres. PCS fibres have an all-silica core and polymer-based cladding, commonly a silicone resin which also serves as a protective layer. They are generally less expensive to manufacture, but are charac-

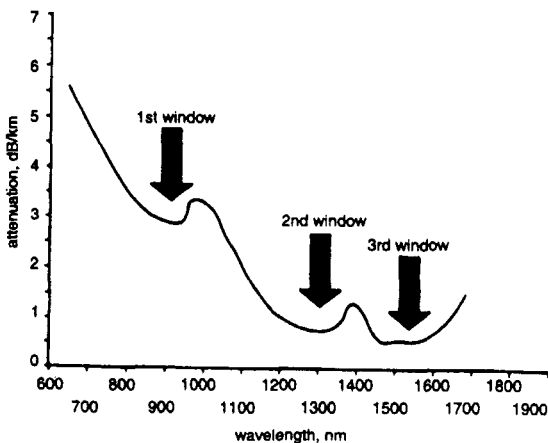


Figure 21.4 *Nominal attenuation against wavelength for silica fibre (showing operating windows)*

terised by higher attenuation and lower bandwidth (as they have a step index) than all-silica fibres, but are used for relatively short data links. All-plastic fibres, generally manufactured from polymethylmethacrylate (PMMA), are the least expensive type. They currently have the highest attenuation of commonly available fibres, and are generally step index. They have applications as 'light pipes' over short distances (metres).

Table 21.1 summarises fibre types and usage.

#### 21.2.4 Fibre protection

The attenuation of a fibre, single- or multi-mode, is increased if it is subjected to bends. Repeated perturbations of the fibre couple light between modes and, if severed, can cause leakage into lossy, radiative modes (those which couple light into the cladding and beyond). In simple terms, excess bending of the fibre causes a light ray on the outside radius of a bend to approach or exceed the critical angle, and light may be lost through the cladding. Such losses are strongly influenced by core and cladding diameters and  $NA$ . A guide to the susceptibility to microbending of a particular multimode fibre type can be made by using the following 'figure of merit' (that is based on step-index analysis but can be used as a general guide):

$$\gamma = K \frac{d_{core}^4}{NA^6 d_{cladding}^6} \quad (21.5)$$

Table 21.1 Fibre types

Type	Core/cladding diameter ( $\mu\text{m}$ )	Typical attenuation (dB/km)	Typical bandwidth (MHz/km)	Applications
<i>All-silica</i>				
Step index multimode	50/125-200/300	3–10 at 850 nm	20	Data links
Graded index multimode	50/125-100/140	3 at 850 nm < 1 at 1300 nm	200–1000	Telecommunications, data links
Single-mode	5/125–10/125	< 0.5 at 1300 nm < 0.25 at 1550 nm	> 1000	Telecommunications, high speed data links
<i>Other</i>				
PCS	50/125-200/300	5–50 at 850 nm	20	Data links
All plastic	50/100-500/1000	> 100	< 20	Light pipes, electrical isolation, short data links

An optical fibre must therefore be protected against radial forces. This is accomplished by mechanically decoupling the fibre from its immediate surroundings, and is commonly achieved by surrounding the fibre with a very low elastic modulus material such as silicone rubber followed by an extruded polymer layer (termed a 'tight' packaged fibre), or by encapsulating the fibre loosely within a polymer tube ('loose' packing). The type of protection depends on the particular application. Note that the pristine surface of an all-silica fibre is always protected during manufacture by a thin ultraviolet (UV) radiation or heat cured polymer layer.

## 21.3 Optical fibre sensing

### 21.3.1 Introduction

Optical fibre sensing is the use of optical fibre based techniques for parameter measurement. The technology differs from that used for telecommunications purposes in that optical elements which are sensitive to external parameters form component parts of the system, whereas in telecommunications systems such external influences are deliberately excluded. Sensing technology is less well developed than telecommunications technology on account of a lower level of commercial drive coupled with arguably the more difficult demands of sensing technology.

The essence of optical fibre technology is that light may be propagated over substantial distances (meters–kilometres) along small diameter ( $\approx 5 \mu\text{m} \rightarrow 1 \text{mm}$ ) transparent filaments in a similar manner to which microwaves are propagated via different modes in rectangular waveguides. By inserting a parameter sensitive optical element into the fibre transmission system the optical signal may be modulated to carry information about the magnitude of the perturbing parameter.

The properties of a lightwave which can be modulated are (Figure 21.5):

- intensity e.g. intensity proportional to the displacement of a reflector from a fibre tip)
- phase (e.g. interferometric measurements)
- polarisation (e.g. Faraday rotation measurement of magnetic field)
- wavelength (e.g. laser Doppler velocity measurement).

These methods may be regarded as primary modulation in the sense that with each method it is ultimately variations in light intensity which are detected. Since intensity is not well conserved in optical fibres (due to variable attenuation effects) some form of intensity referencing is needed, and this in general introduces additional expense and over cumbersome systems. Present sensing research is concerned with overcoming such

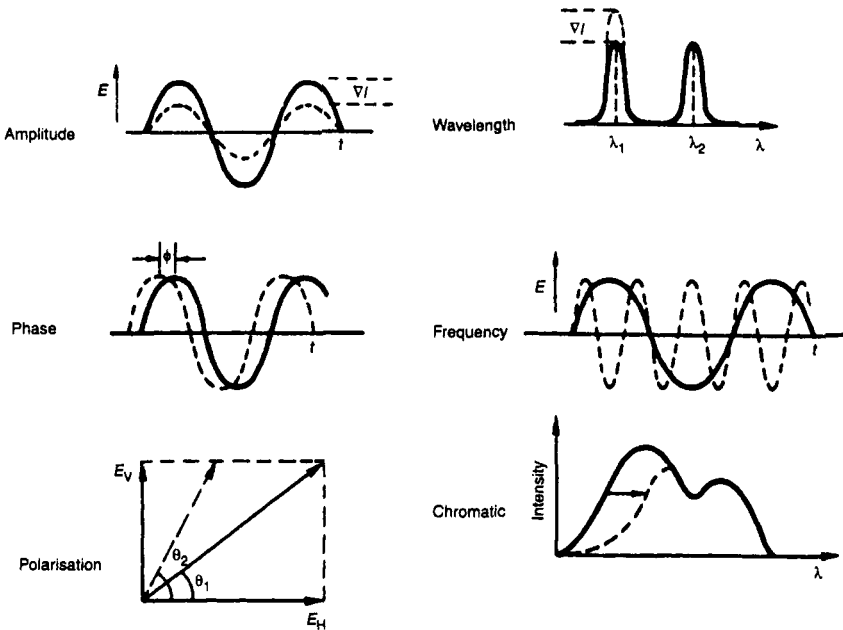


Figure 21.5 Basic optical modulation methods

limitations using a variety of different approaches (e.g. chromatic modulation [1]).

The sensing elements themselves may be one of three types:

- (i) intrinsic, whereby the fibre serves to both transmit and modulate
- (ii) extrinsic, whereby a separate optical element is used for sensing and the fibres are used for transmission to and from the element
- (iii) hybrid, whereby the sensing is nonoptical but signal transmission is by optical fibre following optoelectronic or optomechanical conversion.

Many advantages have been claimed for optical fibre sensors but the reality is that each advantage has an associated engineering problem and these are only currently being addressed. For example, although fibre sensors are

- (i) highly sensitive, they often respond to more than one parameter
- (ii) inherently electrically insulating, they are surface breakdown sensitive at transmission voltages
- (iii) immune to EMI, they are susceptible to mechanical vibration
- (iv) geometrically flexible, even gradual bending over extended lengths causes attenuation
- (v) lightweight, the need for heavier protective sheathing should not be overlooked

- (vi) corrosion resistant, they are susceptible to ionising radiation, microwave heating and solvents.

Despite these difficulties fibre sensing offers considerable potential for measurement in previously unmonitored hazardous environments. By way of illustration a range of parameters which are measurable in principle with the modulation methods listed above is given in Table 21.2.

*21.3.2 Formal representation of an optical fibre sensing system*

The purpose of a sensing system is to seek an output signal  $V$  which is proportional to a measureand  $M$  via a constant which is the sensitivity  $S$ :

$$V = SM \tag{21.6}$$

With an optical fibre system the relationship (eqn 21.6) between the

*Table 21.2 Fibre optic sensor systems and associated optical phenomena (Mitsubishi Electric)*

Measured physical quantity	Optical modulation	Optical phenomenon used	System*	
Current, magnetic field	Polarisation	Faraday effect	DO, FF	
	Phase shift	Interference (magnetic distortion)	FF	
Voltage, electric field	Polarisation	Pockels effect	DO	
	Phase shift	Interference (electric distortion)	FF	
Temperature	Light intensity	Light shading by a plate	DO	
		Changes in light absorption of semiconductors	DO	
	Light intensity, spectrum	Fluorescent radiation	PP	
		Radiation from a heated body	PP	
		Double refraction	DO	
Angular velocity	Polarisation	Sagnac phenomenon	FF	
	Phase shift	Sagnac phenomenon	FF	
Velocity, liquid velocity	Frequency	Doppler effect	PP	
Vibration, acceleration, pressure	Light intensity	Loss due to microbend	FF	
		Light shading by a plate	DO	
		Change of reflection intensity by a diaphragm	DO	
	Polarisation	Photoelasticity	DO	
		Phase shift	Interference (photoelasticity)	FF
		Frequency	Doppler effect	PP

\* DO = discrete optical sensor. PP = pick-up-probe sensor, FF = functional fibre sensors

output  $V$  and modulation  $M_1(\lambda)$  is complicated and depends on parameters such as source power  $P(\lambda)$ , fibre transmission  $T(\lambda)$  and fibre perturbation  $M_2(\lambda)$ , which can be induced by external influences or age:

$$V = q \left[ \int_{\lambda} (P(\lambda) \left[ \int_l T(\lambda) M_2(\lambda) dl \right] R(\lambda) M_1(\lambda) d\lambda) \right]^p \quad (21.7)$$

where  $R(\lambda)$  is the wavelength dependent responsivity of the photodetector and  $\lambda$  is the optical wavelength. It is therefore necessary to seek methods of deployment which minimise or eliminate the disruptive influences.

The two generic approaches and their interconnections which have arguably shown most promise for realising a unified approach to optical fibre sensing – interferometric and chromatic techniques – may be described in terms of eqn 21.7.

### 21.3.2.1 Interferometric sensors

The modulation factor  $M_1(\lambda)$  takes the form

$$M_1(\lambda) \propto \cos^2 \delta(\lambda) \quad (21.8)$$

where  $\delta(\lambda)$  is the phase difference between the interfering light waves of wavelength  $\lambda$ . For instance, if the sensor is based on an interference cavity of thickness  $(\nabla x/2)$  and refractive index  $n$ , then

$$\delta(\lambda) = (\pi n \nabla x) / \lambda \quad (21.9)$$

and the sensor is responsive to any parameter which modifies either the thickness  $\nabla x$  or refractive index  $n$ . Such sensors may involve Fabry Perot cavities, Bragg gratings embedded within the fibres or birefringent materials.

The development of such sensors is concerned with evolving techniques for measuring the interference fringe changes.

### 21.3.2.2 Chromatic sensors

In chromatic sensors the spectral signature  $P(\lambda)$  of the optical signal is modulated by a spectrum changing factor  $M_1(\lambda)$  (eqn 21.7). This may take the form of a change in the wavelength dependent transmittance of the parameter sensing material (e.g. due to absorption or scattering) or indeed due to the wavelength dependence of the optical interference (eqn 21.8). As such, chromatic sensing may, in principle, be regarded as being more widely applicable than monochromatic interferometric sensors, being capable of measuring both physical and chemical parameters.

The detection of signals from chromatic sensors may be achieved using a number  $M$  of photodetectors with nonorthogonal wavelength

responsivities and utilising the Gabor transform type approach described in Chapter 22 for extracting the spectrum defining parameters of dominant wavelength ( $H$ ), effective strength ( $L$ ) and nominal bandwidths ( $S$ ) as the output. In this respect, eqn 21.7 may be regarded as a more complex form of eqn 6, chapter 22 which takes account additionally of optical fibre system artefacts such as wavelength dependent fibre attenuation and sensor modulation.

Earlier forms of chromatic fibre sensing systems relied on an alternative algorithmic processing scheme to the H,L,S method described in Chapter 22, section 22.5.2.3. In this scheme each detector output was intensity normalised according to

$$x_m = \frac{V_m}{\sum_M V_m} \quad (21.10)$$

and a chromaticity map formed in terms of  $x_1, x_2$  for a tristimulus  $M = 3$  system. ( $x_3$  becomes redundant since  $\sum_3 x_m = 1$ .) The special case when  $R_1(\lambda), R_2(\lambda), R_3(\lambda)$  (eqn 21.7) correspond to the responsivities of the human eye leads to the chromaticity map reducing to the CIE diagram of colour science [2, 3].

For most optical fibre sensor applications the use of a distimulus ( $M = 2$ ) rather than a tristimulus ( $M = 3$ ) system is adequate, leading to a simpler signal discrimination in terms of the dominant wavelength ( $\lambda_d$ ) in terms of the ratio of the two detectors' outputs, i.e.

$$\lambda_d = x_1/x_2 = V_1/V_2 \quad (21.11)$$

Most of the experimental results described in Section (21.3.3) below are based on such a distimulus system. Shifts in dominant wavelength ( $\nabla\lambda_d$ ) as small as 0.01 nm are detectable with conventional photodiode detectors using such distimulus system [1].

### *21.3.3 Examples of fibre sensors for high voltage systems monitoring*

In this section we describe examples of optical fibre sensors which have been investigated for monitoring parameters on high voltage equipment and systems. These include sensors for electrical, mechanical, aerodynamic/thermodynamic, mechanical and chemical monitoring. Their particular deployment for high voltage circuit-breaker monitoring is considered and the locations on such from which test results have been obtained are shown on Figure 21.6. Specific parameters which have been tracked include current, voltage, gas pressure, contact stalk temperature, contact travel, particle concentration and arc radiation.

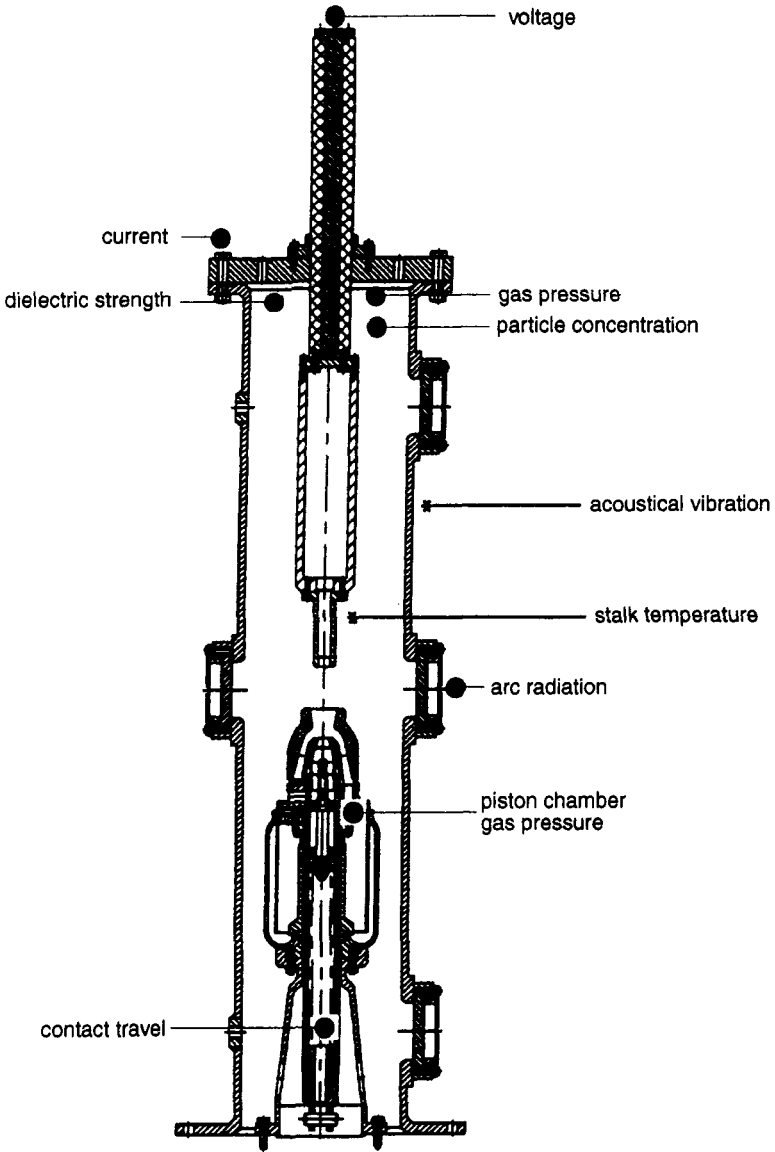
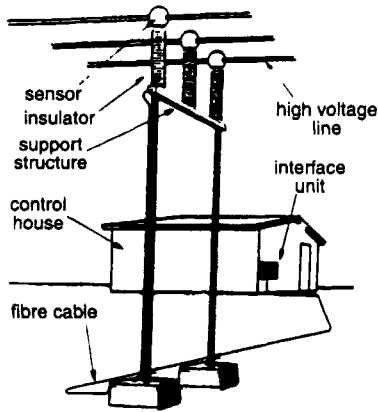


Figure 21.6 Location of various optical fibre sensors on a model high voltage SF<sub>6</sub> circuit-breaker [5]

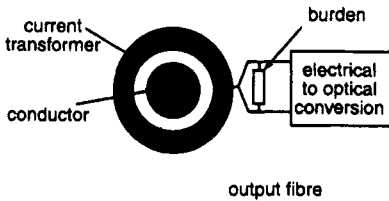
21.3.3.1 Electrical parameters – types of transducers

The range of different forms of optical fibre based current transducers is shown on Figure 21.7 [4] and include the following:

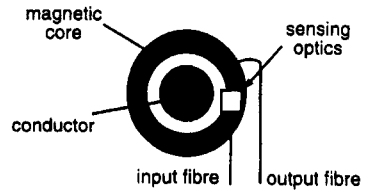
- (i) Extrinsic sensor based on a magneto-optic element which modulates



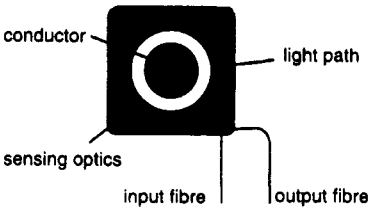
(a) Essential elements of OCT system



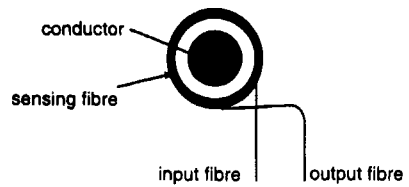
(b) Conventional CT with optical readout



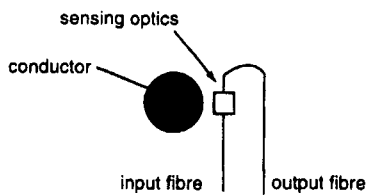
(c) Magnetic concentrator with optical measurement



(d) OCT using bulk optics (e.g. Jackson)



(e) Fibre optics based current measurement (e.g. Rogers)



(f) Witness sensor

Figure 21.7 *Various forms of optical fibre current transducers [4]*

the polarisation of light in proportion to the magnetic field strength produced by the busbar current.

- (ii) Intrinsic sensor based on replacing the extrinsic magneto-optic element by a polarisation preserving fibre wrapped around the current carrying busbar.
- (iii) Bulk extrinsic sensor representing an intermediate case between the purely intrinsic and extrinsic magneto-optic sensors.
- (iv) Magnetic field concentrator based on a magnetic yoke around the current carrying busbar concentrating the B-field into a magneto-optic element in a gap in the concentrator.
- (v) Hybrid optical current transformer in which optical fibre transmission is used to energise and address an electronic current transformer mounted on the high voltage busbar.

Development experiences [4] suggest that for power systems applications the hybrid and magnetic concentrator OCTs perform well.

(a) *Hybrid current transducers*

Hybrid current transducers utilise optical fibres to transmit optical signals and/or power between an optoelectronic receiver based in the control room and a telecommunications type module used to address an electromagnetic current transformer (Figure 21.8) [6].

The ‘telecommunications module’ may in principle be energised either from the powerline itself (which limits measurement resolution and leads to fail safe problems) or by optical energisation via a fibre link.

In either case a paramount need is to minimise the power consumption of the ‘telecommunications module’, which in turn dictates the form of telecommunications encoding used, e.g. pulse frequency modulation, pulse code modulation, etc.

Other problems which have needed to be addressed are:

- long term reliability of components – military based assessment possible

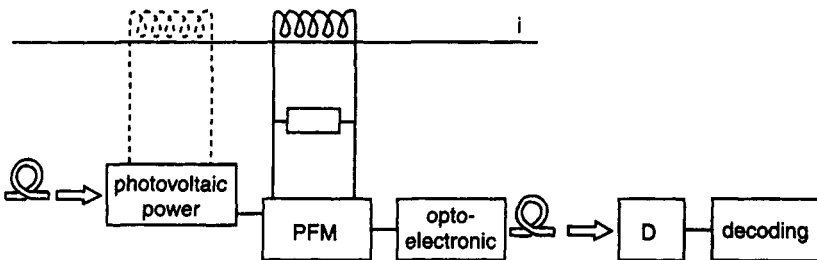


Figure 21.8 Structure of a PFM hybrid current transformer

- temperature stability of the system.
- electromagnetic compatibility of the 'telecommunications module'.

The advantages of the approach include:

- use of established telecommunications techniques
- future evolution benefits from spin-offs from telecoms
- telecommunications module can be multiplexed to transmit other measurements, e.g. temperature, voltage
- compatible with and easily coupled into existing telecommunication fibre systems on EHV transmission network.

Several types of hybrid current transformers have been designed and tested by various organisations world-wide, e.g. ABB, GEC Alsthom (now Alstom), Reyrolle/NGC/University of Liverpool.

Figure 21.9 shows a prototype hybrid CT being used to monitor current flows on the overhead lines powering the crosschannel rail link at Dover, UK.

More recent work has produced a system capable of meeting more onerous specifications than existing electromagnetic current transformers [7].

(b) *Concentrator based Faraday rotation OCT*

The rotation of the plane of polarisation  $\theta$  of a lightwave propagating through a magneto-optic element in a magnetic field of flux density  $B$  is given by

$$\theta = \int V(\lambda) B dl \quad (21.12)$$

where  $V(\lambda)$  is the wavelength dependent Verdet constant of the magneto-optic element, and  $dl$  the optical path traversed in the element.

Since generically it is only possible to measure light intensity, a change in  $\theta$  is measured as the change in intensity of the light passing through a second polarising filter so that only a resolved component of the polarised light wave is transmitted and detected (Figure 21.10), i.e.

$$P_{\theta} = P_{\zeta} \cos^2 \delta \quad (21.13)$$

Problems arise in realising viable engineered systems from the following: (i) the constant of proportionality between  $\theta$  and  $B$  (Verdet constant  $V$ ) for high  $V$  materials varies significantly with temperature; (ii)  $\theta$  for high  $V$  materials is also strongly dependent on stress, making the electro-optic element highly sensitive to mechanical vibration.

Optical intensity is also affected by external factors, e.g. source ageing.

The variation of  $\theta$  with  $B$  is cyclical, so the range of operation is governed by the range within which  $\theta(B)$  has linearity within the required specifications.

Research has therefore been directed towards overcoming these

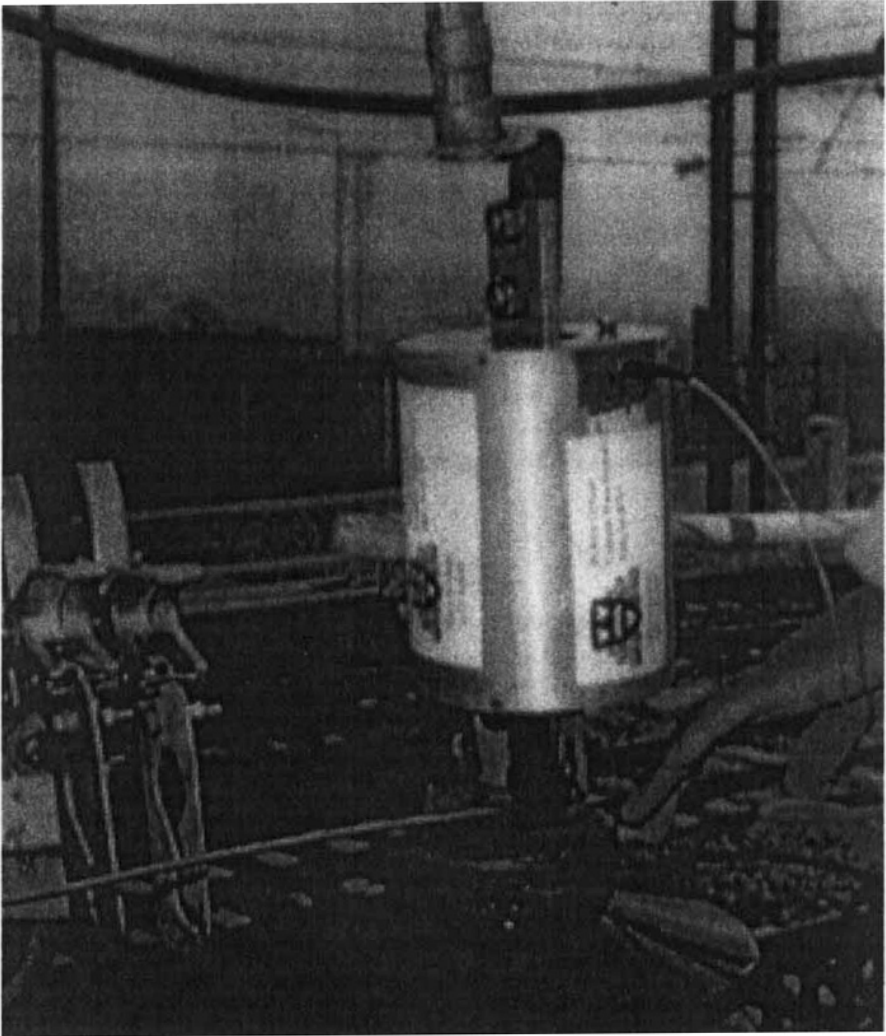


*Figure 21.9 A hybrid current transformer mounted for field use*

limitations. To aid this the following points are worth noting: (i) polarising filter action is limited to the visible range so that the infra-red range may be used for referencing the optical signal; (ii) the Verdet constant varies with the wavelength  $\lambda$ , leading to additional possibilities for improving measurement linearity.

Various chromatic modulation forms of the concentrator OCT have been described [8] which seek to overcome the practical limitations described above. These chromatic schemes variously use unpolarised infra-red light as a reference for the polarised visible light, the wavelength

dependence of the Verdet constant leading to different wavelengths having their planes of polarisation rotated by different amounts, and the use of a quartz birefringent element for wavelength encoding the polarised light.

A typical performance of a chromatic Faraday rotation OCT is shown on Table 21.3.

(c) *Electro-optic voltage transducers*

Electro-optic transducers sense changes in voltage via the effect of the associated electric field on the polarisation of light propagating through an electro-optic element. In such elements light propagates via two contrary circularly polarised waves which when recombined constitute a linearly polarised wave (Figure 21.11). The phase difference between the two circularly polarised waves varies with the magnitude of the electric field, as therefore does the orientation of the output

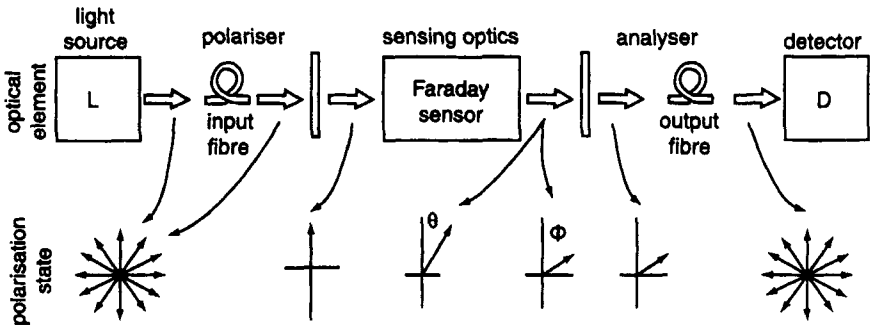


Figure 21.10 Typical arrangement of optical components and polarisation components in Faraday sensor

Table 21.3 Typical Faraday rotation OCT performance

	Chromatic modulation*	DC referenced †
Accuracy, %	<1	-1.7-6
Sensitivity, A	0.5	10?
Range, kA <sub>RMS</sub>	1	2
Frequency response (receiver limited)	DC-1 kHz	Not DC
Temperature sensitivity	≪ 100 ppm/°C	-1.5% (-10-80 °C)
Vibrational sensitivity	None detected	?
Optical fibre length, m	-200	?

\* - NGC/Reyrolle/University of Liverpool

† - Chubu Electric Power, Japan (1994) [9]

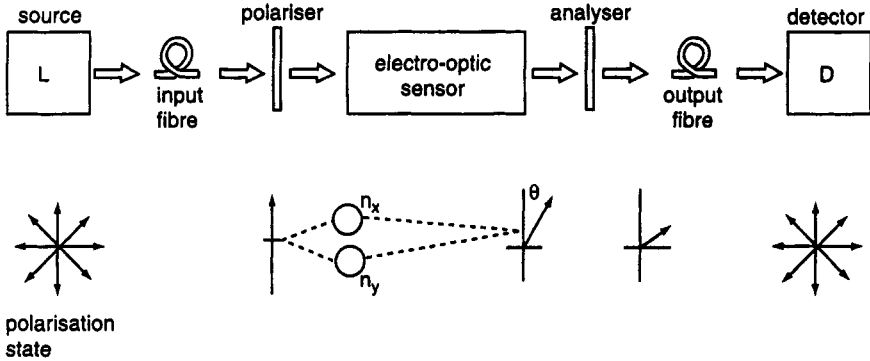


Figure 21.11 Electro-optic sensing system

linearly polarised wave. Thus the output optical power varies with the phase difference between the two circularly polarised waves, according to

$$P_o = P_i \sin^2 (\delta/2) \tag{21.14}$$

where

$$\delta = \frac{2\pi}{\lambda_0} n_o 3 T_{ij} V \tag{21.15}$$

$\lambda_0$  = optical wavelength,  $n_o$  = refractive index under zero  $E$ -field conditions,  $T_{ij}$  is the linear electro-optic coefficient of the sensing element (Pockels effect) and  $V$  the voltage. Thus the optical modulation is described by the interference type modulation factor  $M_1(\lambda)$  from eqn (21.8).

Similar problems to magneto-optic elements exist with electro-optic elements in having high sensitivities to temperature and to vibration. In addition there are difficulties in exposing miniature electro-optic elements to  $E$ -fields which are representative of the voltage levels (145, 420 kV) found at distribution and transmission levels without exposure to electrical breakdown across the electro-optic element.

### 21.3.3.2 Mechanical parameters

Mechanically based malfunctions have been claimed to be responsible for the majority of faults which occur on circuit-breakers and so the monitoring of such parameters would appear to have a high priority. The requirement is to have the capability of monitoring such mechanical parameters during the process of current interruption being undertaken by the circuit-breaker when it is mechanically active, i.e. the electrical contacts are being mechanically parted, and in puffer circuit-breakers gas compression is being achieved by piston action.

Useful mechanical parameters to monitor during this operation are the contact travel/velocity and the mechanical vibration of the circuit-breaker assembly.

One type of optical fibre contact travel sensor consists of a computer designed scale along whose length the dominant wavelength is arranged to vary between possible limits in a linear manner [10]. To achieve such a linear performance a dot matrix pattern is used the density of which causes the proportion of visible and infra-red light reaching the chromatic detectors to vary (Figure 16.12(a)). The dominant wavelength ( $\lambda_d$ ) is related to the percentage greyness of the dot pattern ( $x$ ) according to [5]

$$\lambda_d = \lambda_s + AX - BX^2 + CX^3 \quad (21.16)$$

where  $\lambda_s$  is the unmodulated dominant wavelength and  $A$ ,  $B$ ,  $C$  are constants determined by the optics of a particular system.

To monitor contact travel over 200 mm with acceptable resolution, two scales operating in parallel are required – a coarse scale producing a stepped change in dominant wavelength (Figure 21.12a) extending the full length of the 200 mm travel and a fine scale producing a periodic modulation (Figure 21.12b) with a period of about 20% of the full scale.

In practice the scale is mounted on a polished stainless steel reflector covered with a chemically inert protective film and mounted on the contact stalk (Figure 21.13a). Imperfections on the reflective surface which produce 15% error in optical intensity only produced 0.5% error in dominant wavelength. Likewise rotation of the contact stalk during circuit-breaker operation ( $\sim \pm 3^\circ$ ) produced a 16% change in optical intensity but only 0.8% change in chromaticity. The superior performance of the chromatic approach yielded an overall dynamic resolution of 1% under real operating conditions.

Installation of the transducer on a 145 kV puffer circuit-breaker has led to travel records of the form shown in Figure 21.13b which are highly repeatable from operation to operation at fault currents of several tens of kiloamperes [5].

Mechanical vibration measurements have been undertaken opto-acoustically with a fibredyne interferometer. The fibredyne interferometer detects acoustical signals via the effect of the rarefactions and compressions of a soundwave on the refractive index of the core of an optical fibre [11]. These small changes in refractive index modulate the interference of various optical propagation modes within the fibre, so causing detailed changes in the far-field interference pattern (speckle) from the fibre [11]. Through the use of carefully chosen spatial filters, fluctuations in the speckle pattern can be monitored via a simple photodiode detector. By winding an optical fibre around part of the circuit-breaker structure acoustical and mechanical vibrations produced by the arcing

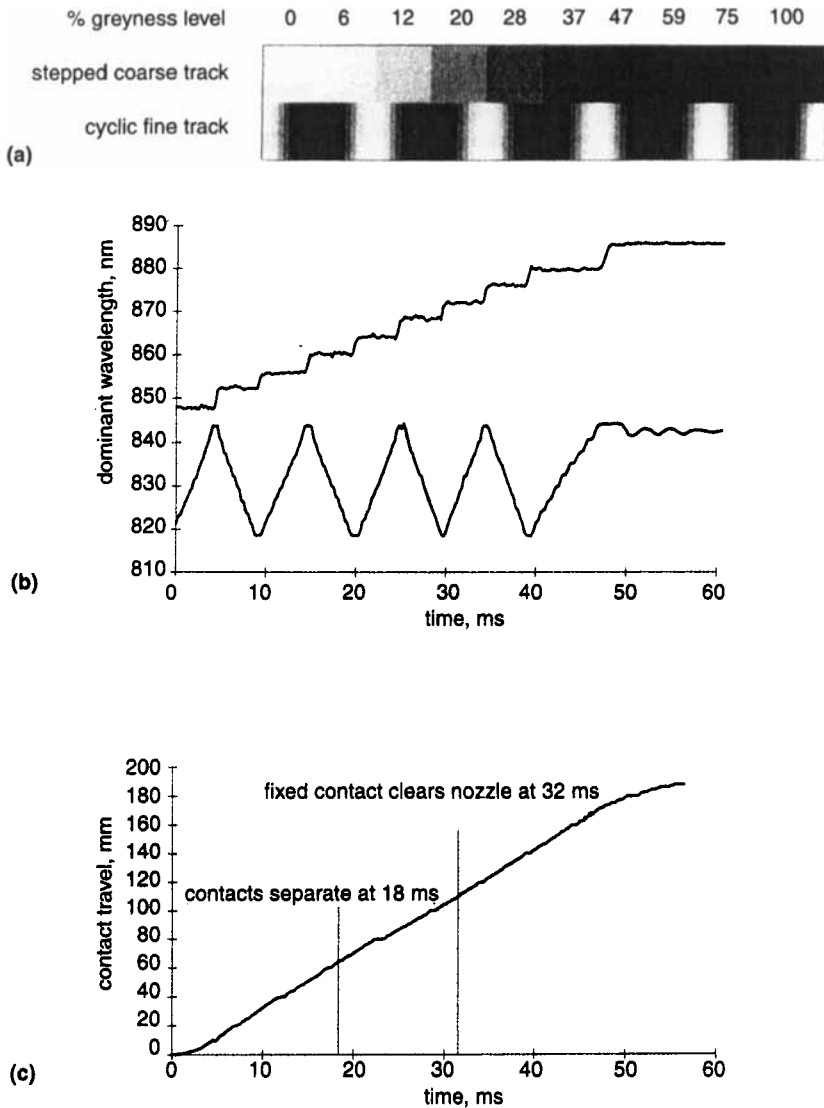


Figure 21.12 Chromatically based optical fibre linear travel recorder [5]  
 (a) Dual track chromatic scales with linearised dot density deposition  
 (b) Dominant wavelength variation for a linear traverse of the scale  
 (c) Typical contact travel: time characteristic

and other mechanical effects associated with the operation of the breaker (e.g. piston and contact movement, fluid compressing pump, etc.) can be conveniently monitored.

Figure 21.14a shows two time dependent acoustical signals which are representative of sets of records obtained during the operation of an SF<sub>6</sub>

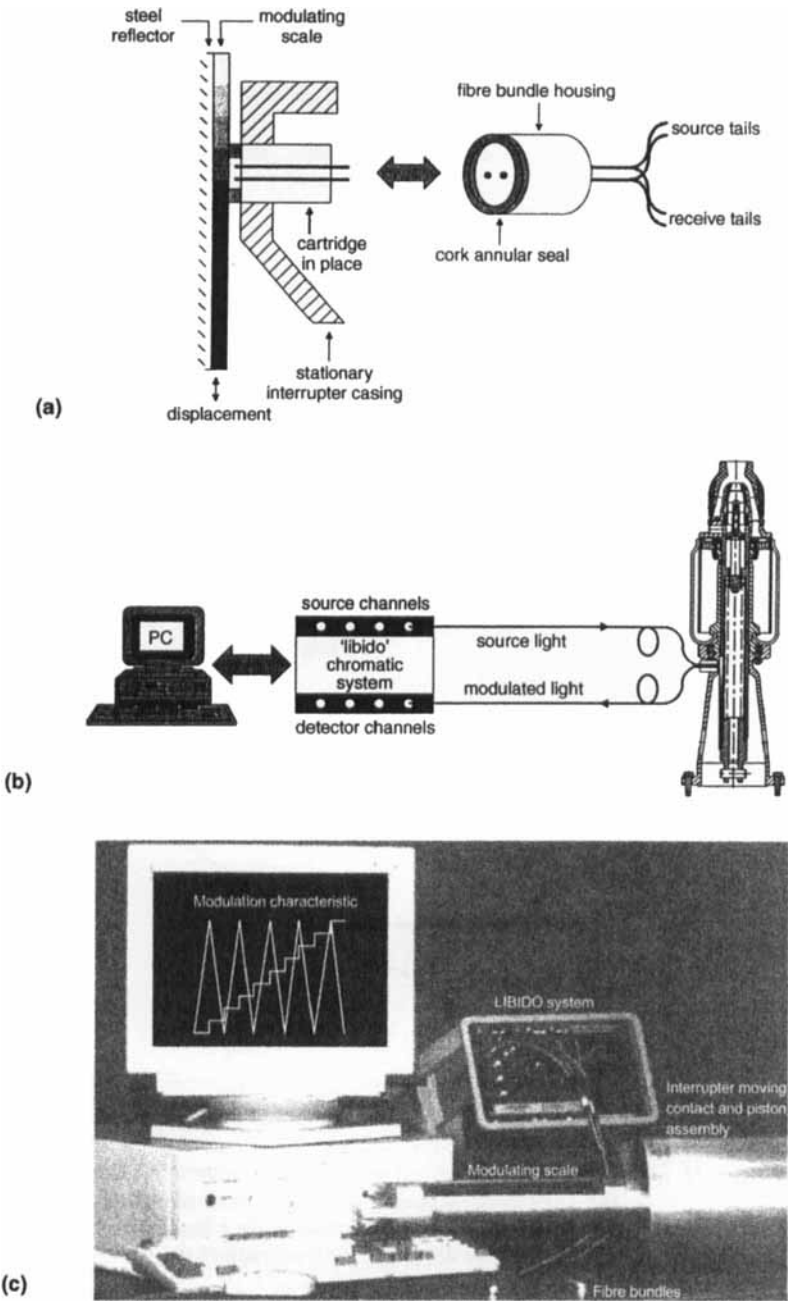


Figure 21.13 Structure of optical fibre linear travel recorder system [5]  
 (a) Structure of the sensing head  
 (b) Schematic diagram of the fibre system  
 (c) System photograph [5]

puffer circuit-breaker under different fault current arcing conditions. A bandpass frequency of 8–10 kHz was used for these particular tests.

These two records represent two distinct conditions investigated, namely operation with no fault current flowing (no load) and operation with a fault current of 31.1 kA peak at 50 Hz. (Other results were obtained for fault currents of 14.3 44.1, 59.5 kA peak).

The records cover a total time duration of 100 ms with the contact and piston movement limited to the time interval 15–55 ms and the main arcing to the interval 25–34 ms. The main contact movement period prior to mechanism buffering is clear from the lower amplitude signals duration on the no load record. The more pronounced vibrations during this contact moving phase with fault current flow is apparent from the 31.1 kA record, but distinction from the buffering phase is now less discernible.

Fourier transform analysis highlights different spectral features of the vibration signals under different current operating conditions (14.3, 44.1, 59.5 kA) but does not easily yield a ‘figure of merit’ since changes are distributed over extensive parts of the acoustical spectrum (Figure 21.14*b*). On the other hand, analysis of the signals via the time domain based Gabor transforms (chapter 22, section 22.5.3) yields clear quantitative trends with fault current in dominant time (hue angle), effective time duration (saturation) and nominal energy (lightness) (Figure 21.14*c*), so demonstrating the power of the chromatic methodology for discriminating signals in a quantitative manner. Analysis of other features from such acoustical records using the chromatic approach yields deeper levels of information regarding the mechanical operation of the circuit-breaker (e.g. hydraulic drive pressure), as already described in Chapter 22.

### *21.3.3.3 Aerodynamic and thermodynamic monitoring*

The control of gas pressurisation and a knowledge of heating effects provide powerful means of monitoring circuit-breaker behaviour provided that these can be undertaken during switching operation when arcing occurs and when fibre sensing provides a measurement means which would otherwise be difficult to achieve. The gas pressure in the piston compression chamber of a puffer interrupter and the temperature of the contact stalk can both be measured via a Fabry-Pérot cavity interferometer addressed polychromatically via optical fibre transmission. As such the technique is illustrative of how chromatic modulation defined by eqns 21.10 and 21.11 and interferometric sensing defined by eqns 21.8 and 21.9 may be used combinatorially to provide an effective sensing system for such a difficult operating environment.

A fibre addressed Fabry-Pérot cavity consists of a silicon wafer into which a cavity is etched and with a semi-reflective glass plate bonded to cover the cavity (Figure 21.15) [5]. Two multimode step-index fibres for delivering and receiving the polychromatic light are butted to the glass

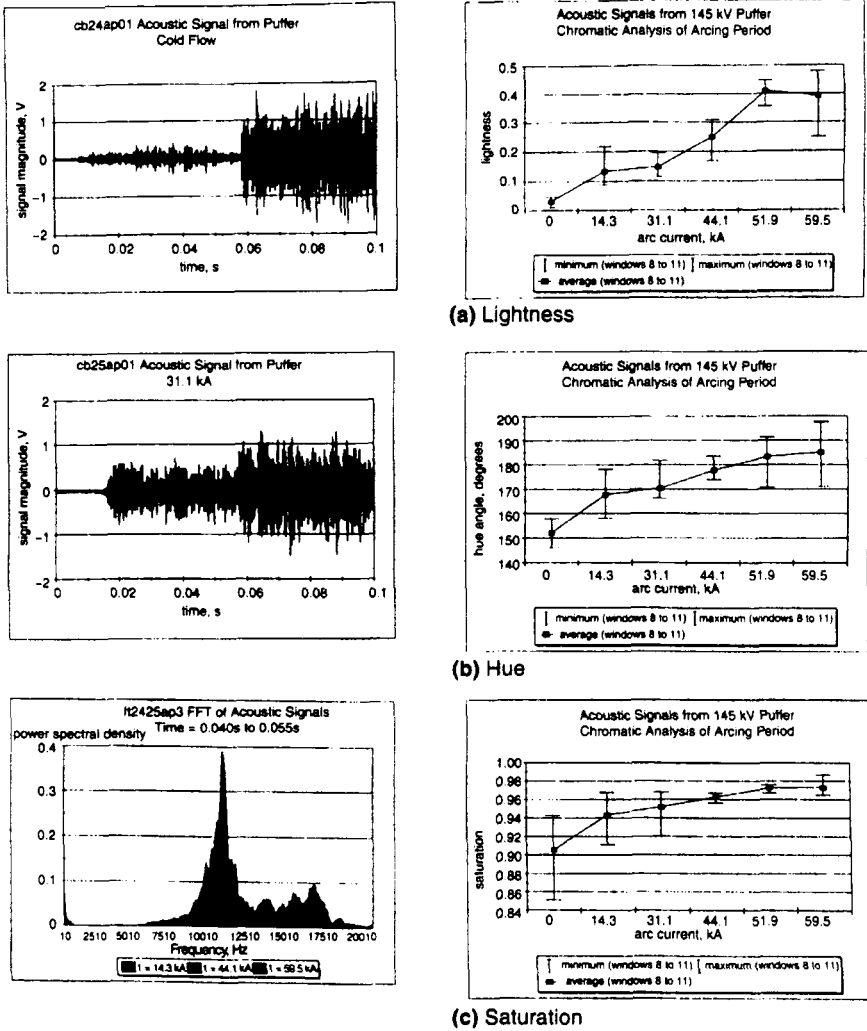


Figure 21.14 Optoacoustic vibration monitoring [12]

- (a) Typical time variation of acoustic signals from an SF<sub>6</sub> puffer circuit-breaker without a fault current and with a 31.1 kA fault
- (b) Power spectral density curves for acoustical signals from an SF<sub>6</sub> puffer circuit-breaker for part of the fault current arcing period
- (c) Signal discrimination in terms of time window compressed coordinates L,H,S

plate. The depth of the cavity (~ 0.3–1 μm) is monitored via the optical interference between light reflected from the glass plate surface and that reflected from the silicon surface on the other side of the cavity leading to the phase difference defined by eqn 21.8. The outer surface of the silicon wafer is coated with aluminium to prevent infra-red radiation from the

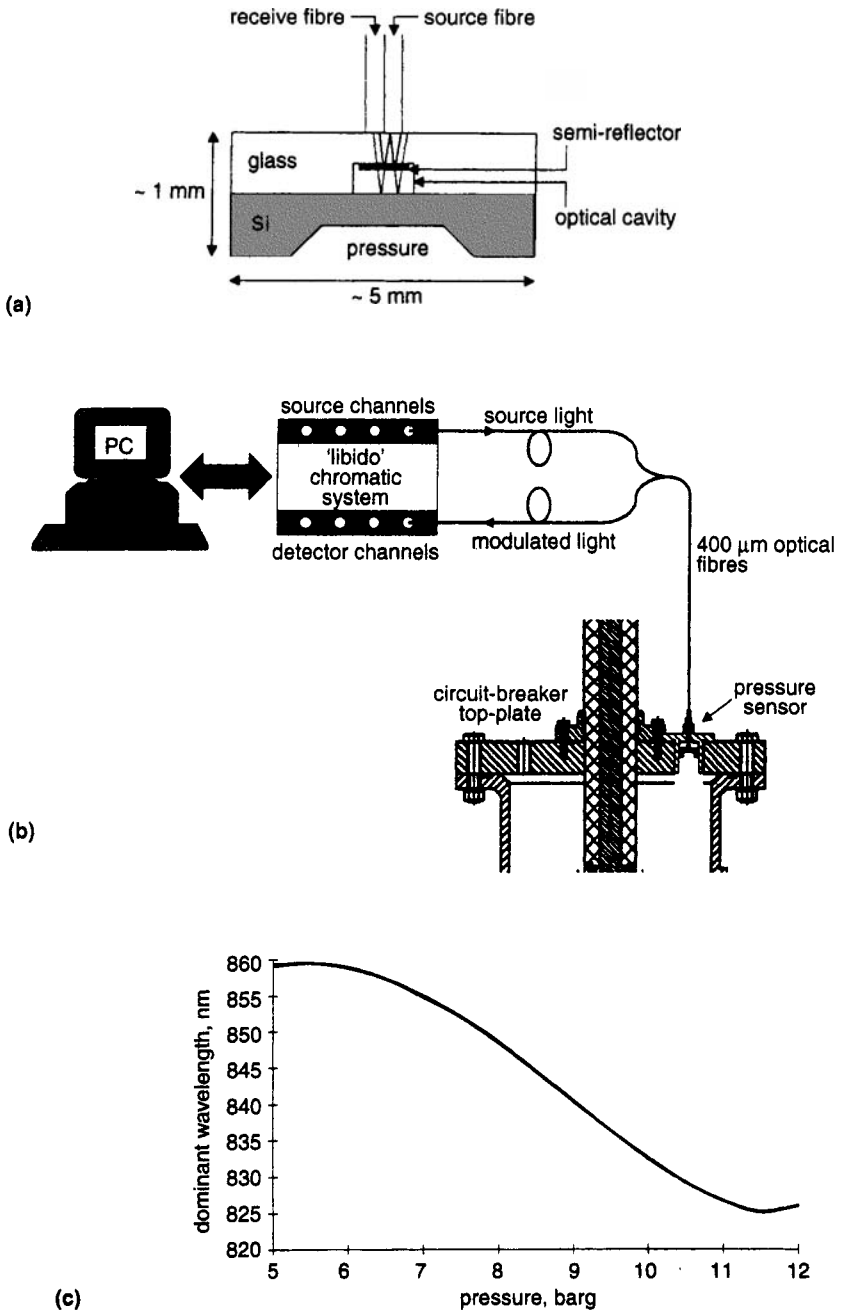
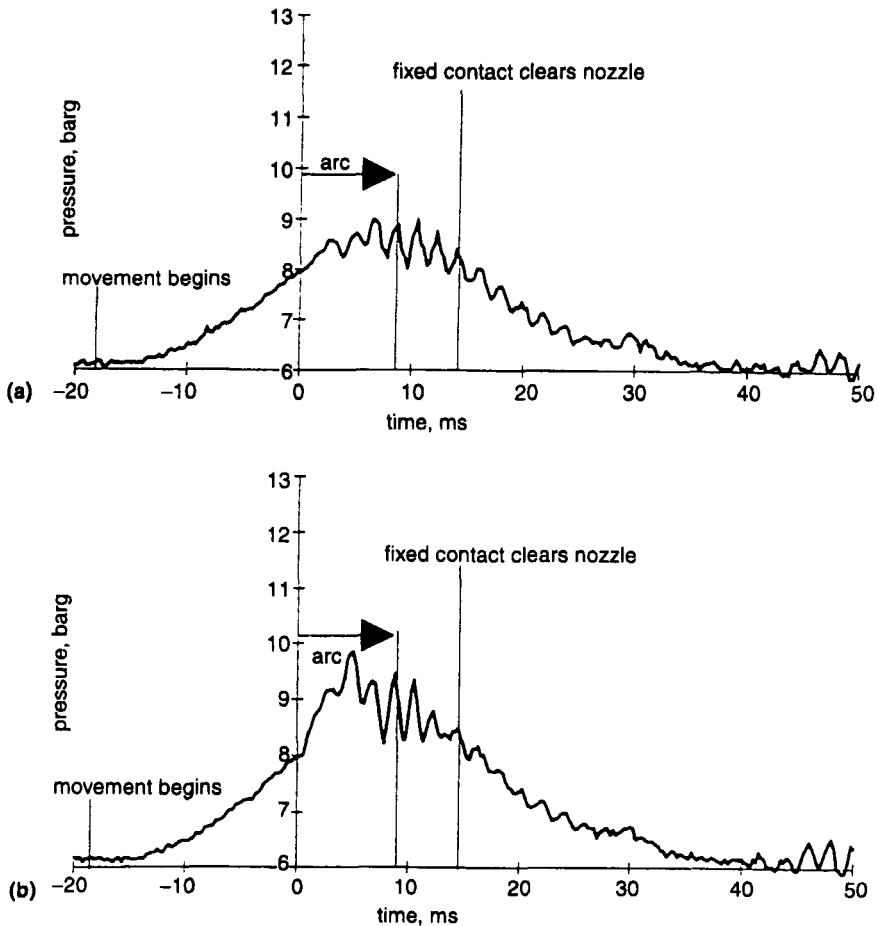


Figure 21.15 Chromatic Fabry-Pérot pressure sensor [5]  
 (a) Sensor structure  
 (b) Optical fibre measurement system  
 (c) Calibration curve

electric arc formed during current interruption being transmitted into the cavity via the silicon.

In the case of the gas pressure sensor the thickness of the silicon wafer is adjusted during manufacture to flex under pressure to give the required measurement dynamic range. A typical calibration curve for dominant wavelength against pressure is given in Figure 21.15c showing the  $\cos^2$  nature of the curve. The dynamic range is defined by the range of pressure over which the curve has an acceptable degree of linearity. Some typical pressure transients measured in the piston chamber of an SF<sub>6</sub> puffer interrupter are shown in Figure 21.16 during the interruption of fault currents of 5 and 15 kA peak [5].



*Figure 21.16 Time variation of piston chamber pressures [5] measured with the chromatic Fabry-Pérot sensor*  
 (a) 5 kA fault current  
 (b) 15 kA fault current

In the case of the contact stalk temperature sensor the silicon wafer is made sufficiently thick so as not to flex under pressure and the glass plate is arranged to have a thermal expansion coefficient which is very different from that of the silicon. Temperature changes produce internal stresses which lead to changes in the cavity depth and which are addressed via polychromatic interference as in the case of the pressure sensor. A typical dominant wavelength: temperature calibration curve is given in Figure 21.17 showing a low level of hysteresis between heating and cooling cycles. A resolution of 0.1% of full scale is shown to be achievable.

Test results obtained with such a probe embedded in the contact stalk of a puffer interrupter 13 cm from the contact tip (Figure 21.18) have been obtained during and after the interruption of a range of different levels of fault currents [14]. These show that temperature changes of up to about 11 deg.C occur following arcing for peak currents above about 17 kA. The tests at 60 kA show that two half-cycle arcing produces a prolonged thermal transient compared with single half-cycle arcing. The contact temperature returns to ambient in about 0.5 s.

#### 21.3.3.4 Chemical and plasma monitoring

The chromatic modulation approach enables the optical emission from the arc plasma during current interruption to be monitored along with the concentration of particulate material formed during complex chemical reactions in the arc plasma using a single optical fibre probe. Particle concentration may be obtained by monitoring the change in the spectral signature of polychromatic light [5].

Information about the spectral signature of the optical emission from the electric arc formed during current interruption in an SF<sub>6</sub> interrupter

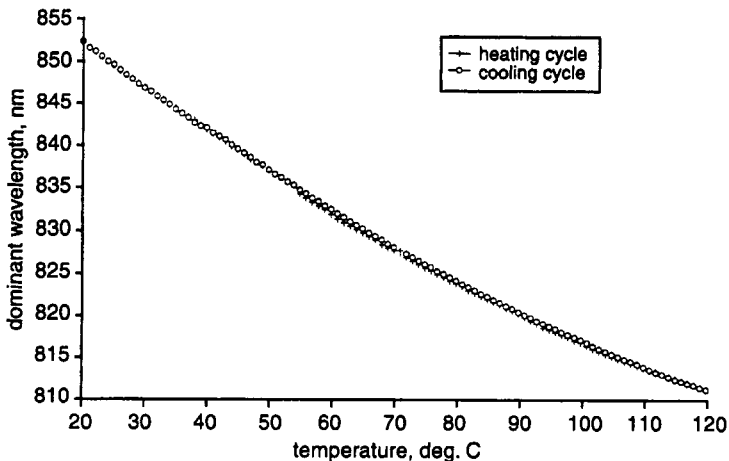


Figure 21.17 Chromatic Fabry-Pérot temperature transducer [13]: dominant wavelength: temperature calibration curve

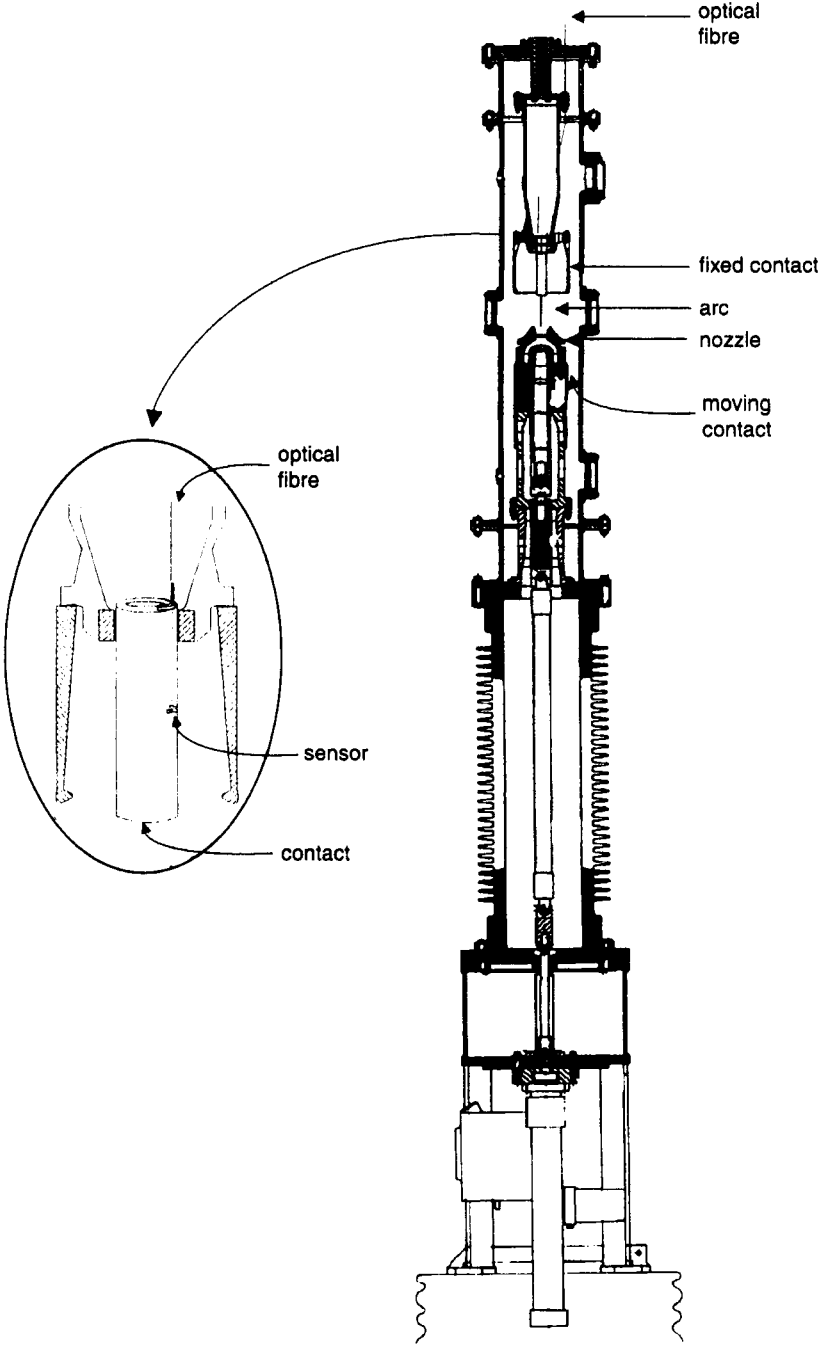


Figure 21.18 Location of the chromatic Fabry-Pérot sensor of Figure 21.17 within a 145 kV circuit-breaker

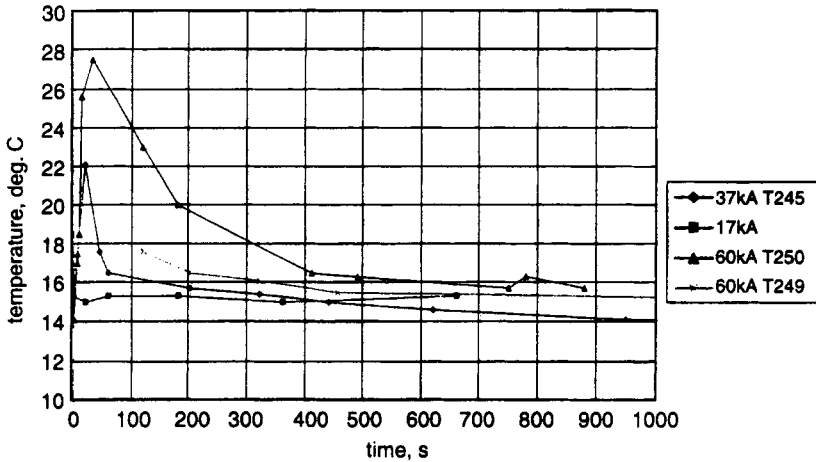


Figure 21.19 Contact temperature after fault current interruption [14]

may be obtained by comparing the emission with that of a known polychromatic source. Monitoring the output optical signal chromatically leads to the arc signature being quantified by the measured dominant wavelength shift. An optical fibre probe for achieving such monitoring is shown on Figure 21.20a and involves transmitting a broad collimated polychromatic beam across a monitoring gap between two optical fibres. Light scattered and reflected from the electric arc plasma within an interrupter is collected by the receiving fibre superimposed on the known collimated beam. The signature of the arc emission is then obtained as a shift in the dominant wavelength of the superimposed optical signals. Typical time variations of the dominant wavelength of such superimposed signals are shown in Figure 21.20b for a number of fault arc currents in the range 2 to 15 kA. The shift in dominant wavelength with current is mainly due to the intensity of the arc plasma emission increasing so that the technique provides a convenient method for intensity referenced monitoring [15, 16].

Particle concentration monitoring may be achieved with the same optical fibre sensor arrangement as shown in Figure 21.20a. The particle concentration is obtained by monitoring the change in the spectral signature of polychromatic light produced by scattering by micron sized particles. The intensity of the forward scattered light  $I_F$  is a complex function of optical wavelength ( $\lambda$ ), particle radius ( $R_p$ ) and particle concentration ( $N$ ) governed by [17], [1]:

$$I_F = I_0(1 - CN\alpha^2[\lambda^4 R_p^2]^{-1})$$

where  $I_F$  is the intensity of the forward scattered light,  $I_0$  the incident intensity,  $\alpha$  the particle polarisability and  $C$  a constant.

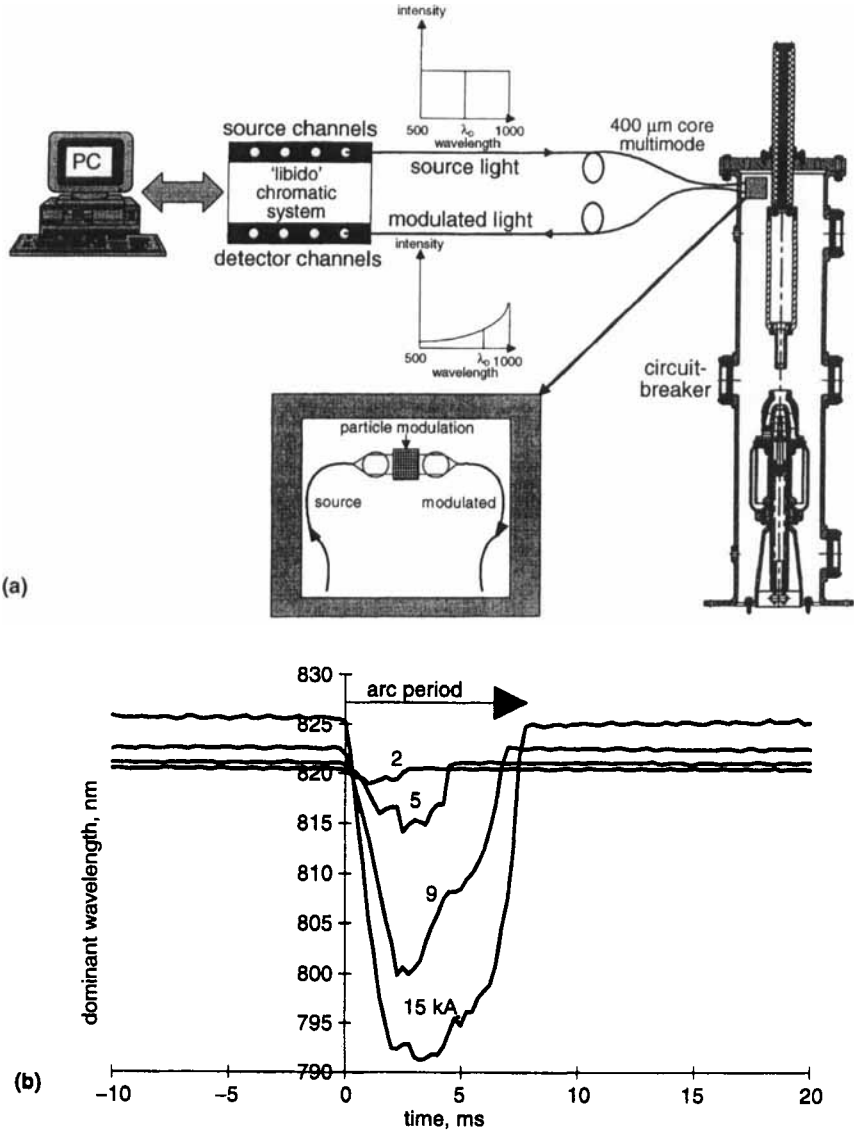


Figure 21.20 Plasma and particulate chromatic monitoring [5]

(a) Sensor structure and location in circuit-breaker

(b) Arc optical emission and scattered light

The implication is that the wavelength of the forward scattered light is a function of the fractional volume of micron sized particles  $NR_p^2/R_A^2$ , where  $R_A$  is the radius of the cylindrical volume being optically addressed. Thus the light detected in the forward direction will contain forward scattered light mixed with the range of wavelengths contained in

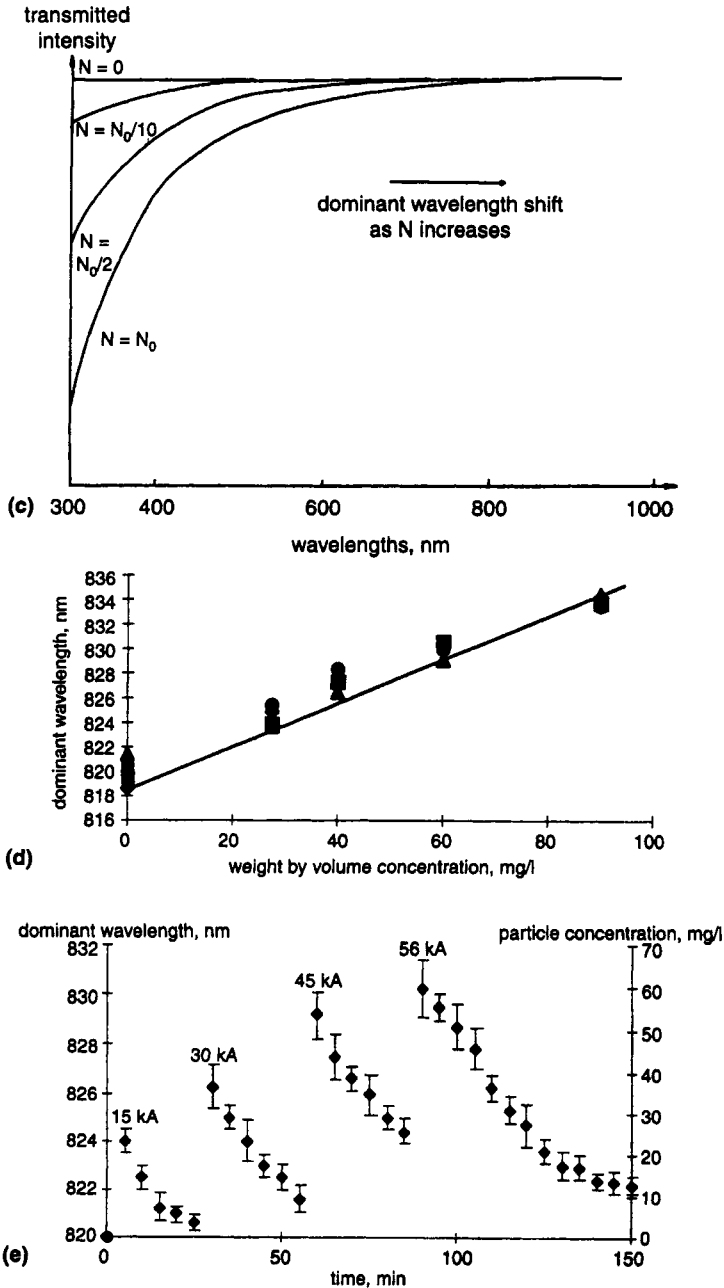


Figure 21.20 continued

- (c) Effect of particle concentration on transmitted intensity for the case of Rayleigh scattering (Beaven [17])
- (d) Calibration curve for optical fibre particle concentration monitor
- (e) Time variation of dominant wavelength from the OFPCM for a range of high fault currents

the polychromatic addressing light beam and weighted towards a particular value governed by  $(NR^2_\mu/R^2_A)$ .

The change in the forward scattered light intensity is shown as a function of wavelength on Figure 21.20c and indicates that a dominant wavelength shift should occur if the output was monitored chromatically. Such particle concentration changes should therefore be measurable in principle with the same optical fibre sensor probe shown in Figure 21.20a.

Calibration of such a probe with known quantities of well dispersed particles gathered from arcing tests in SF<sub>6</sub> yields the dominant wavelength: particle concentration curve of Figure 21.20d which shows a high degree of linear correlation. Test results obtained with this probe using the calibration curve for a 145 kV 63 kA SF<sub>6</sub> puffer circuit-breaker are given in Figure 21.20e for a continuous sequence of tests whereby peak fault currents of 15, 30, 45 and 56 kA were monitored.

The results show that the amount of particulate material produced by arcing increases from about 23 mg/l at 15 kA to about 60 mg/l at 56 kA. (The results are for a full half-cycle of arcing at 50 Hz.) The results also show the rate at which the particulate material settles after arcing. The initial rate of decay of the particulate concentration following arcing appears to be similar for each peak fault current. These settling times are of the order of about 25 min at 15 kA and 60 min at 56 kA.

Thus the results of Figure 21.20b and 21.20e show that the chromatically addressed optical fibre probe serves the dual function of providing arc emission information on a short timescale ( $\approx 10$  ms) and particle concentration information on longer timescales ( $t > 10$  ms).

### 21.3.4 Conclusions

The scope of optical fibre sensing for high voltage equipment and systems monitoring has been illustrated with respect to circuit-breaker applications. The techniques are equally applicable to other high voltage equipment such as transformers. Already the use of optical fibre distributed sensors for monitoring temperatures and hot spots is apparent in relation to the windings of transformers.

A number of extensions of the fibre sensor types described above for circuit-breakers are possible to other equipment. For instance, the optoacoustic fibredyne interferometer (Section 21.3.3.2) has been deployed for monitoring partial discharges in gas insulated systems [11] (Section 22.4.5.1, Coventry) and in power cables [18]. Modified forms of the chromatic particle monitor have already been utilised for oil monitoring in the semiconductor industry and for kerosene monitoring in the nuclear industry [19] and have the potential for application to transformer oil monitoring.

The chromatic approach to optical fibre sensing is synergetic with the broader issue of intelligent monitoring discussed in Chapter 22 via the

utilisation of the chromatic processing for extracting information about complex systems operation. The methodology therefore permeates through the intelligent monitoring system illustrating how intelligence may be distributed therein.

## 21.4 Acknowledgments

Much of the work reported here was supported by EPSRC, Reyrolle Switchgear, NGC, Lucas Technology and the European Social Fund. A number of researchers have contributed to the work, including Dr P.C. Russell, Dr J.W. Spencer, Dr L.T. Isaac, Dr J. Cosgrave, Mr J. Humphries and D. Messent – their efforts are much appreciated.

## 21.5 References

- 1 JONES, G.R. and RUSSELL, P.C.: 'Chromatic modulation based metrology', *Pure Appl. Opt.*, 1993, **2**, pp. 87–110
- 2 ROSSOTTI, H.: 'Colour' (Princeton University Press, New Jersey, 1983)
- 3 CIE (Commission International de Eclairage): International Lighting Vocabulary, 3rd Edition, Publication CIE No. 17 (E-1.1), Bureau Central de la CIE, Paris, 1970
- 4 IEEE Working Group: 'Optical current transducers for power systems: a review', *IEEE Trans. Power Deliv.*, 1994, **9**, (4), pp. 1778–1788
- 5 ISAAC, L.T.: 'Puffer circuit-breaker diagnostics using novel optical fibre sensors'. PhD Thesis, University of Liverpool, 1997
- 6 PILLING, N., HOLMES, R. and JONES, G.R.: 'Hybrid current measurement system', *Electron. Lett.*, 1993, **5**, pp. 1049–1051
- 7 DONALDSON, E.: 'Hybrid optical current transformer'. M.Phil. Thesis, University of Liverpool, 1999
- 8 JONES, G.R., LI, G., SPENCER, J.W., ASPEY, R.A. and KONG, M.G.: 'Faraday current sensing employing chromatic modulation', *Opt. Commun.*, 1998, **145**, pp. 203–212
- 9 HASEGAWA, Y., ICHIKAWA, Y., KATSUKAWA, H. TAMAKA, N. and SAKURAIY, K.: 'Development of a new type of optical transducer for measuring fault current', *IEEE Trans. Power Deliv.*, 1994, **9**, (3), pp. 1245–1250
- 10 ISAAC, L.T., SPENCER, J.W., JONES, G.R., JONES, C., HALL, W.B. and TAYLOR, B.: 'Live monitoring of contact travel on EHV circuit-breakers using a novel optical fibre technique'. Proc XIth Int. Conf. on *Gas discharges and their application*, Tokyo, 1995, vol. II, pp. 238–241
- 11 COSGRAVE, J.A., VOURDAS, A., JONES, G.R., SPENCER, J.W., MURPHY, M.M. and WILSON, A.: 'Acoustic monitoring of partial discharges in gas insulated substations using optical sensors', *IEE Proc. A*, 1993, **140**, (5), pp. 369–374
- 12 COSGRAVE, J. HUMPHRIES, J.E., SPENCER, J.W., JONES, G.R., RUSSELL, P.C., HALL, W.B. and LEWIS, K.G.: 'Chromaticity character-

- isation of optoacoustic signals from fault current arcs in high voltage circuit-breakers'. Proc. XIIth Int. Conf. on *Gas discharges and their applications*, Greifswald, 1997
- 13 MESSENT, D.N., SINGH, P.T., HUMPHRIES, J.E., SPENCER, J.W., JONES, G.R., LEWIS, K.G. and HALL, W.B.: 'Optical fibre measurement of contact stalk temperature in an SF<sub>6</sub> circuit-breaker following fault current arcing'. Proc. XIIth Int. Conf. on *Gas discharges and their applications*, Greifswald, 1997
  - 14 MESSENT, D.: Private communication, 1997
  - 15 ISAAC, L.T., JONES, G.R., HUMPHRIES, J.E., SPENCER, J.W. and HALL, W.B.: 'Monitoring particle concentrations produced by arcing in SF<sub>6</sub> circuit-breakers using a chromatic modulation probe', *IEE Proc. Sci. Meas. Technol.*, 1999, **146**, 4, pp. 199–204
  - 16 ISAAC, L.T., SPENCER, J.W., HUMPHRIES, J., JONES, G.R. and HALL, W.B.: 'Particle formation by SF<sub>6</sub> circuit-breaker arcs'. Proc. XIIth Int. Conf. on *Gas discharges and their applications*, Greifswald, 1997
  - 17 BEAVAN, C.M.: 'Colour measurement in optical metrology'. PhD Thesis, University of Liverpool, 1989
  - 18 PARADA, S., SPENCER, J.W., JONES, G.R., CUNNINGHAM, J. and RICHEY, K.: 'An optical fibre based technique for determining the electrical status of a 3-phase 11 kV belted power cable'. Proc. 3rd Int. Conf. on *Electrical contacts, arcs, apparatus and their applications* (IC-ECAAA), Xian, P.R. China, 1997
  - 19 KHANDAKER I.I., GLAVAS, E. and JONES, G.R.: 'A fibre-optic oil condition monitor based on chromatic modulation', *Meas. Sci. Technol.* 1993, **4**, pp. 608–613